ACS OMEGA

http://pubs.acs.org/journal/acsodf

Article

High-Pressure Behavior and Disorder for Ag_2ZnSnS_4 and Ag_2CdSnS_4

Tim Küllmey,* Jakob Hein, Eva M. Heppke, Ilias Efthimiopoulos, and Beate Paulus

Cite This: *ACS Omega* 2021, 6, 27387−27395

Read Online

ACCESS | Metrics & More | Article Recommendations | Supporting Information

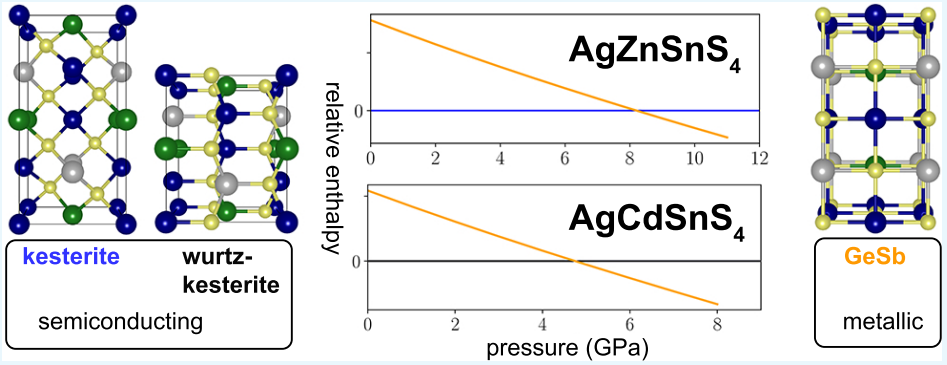

ABSTRACT: We carried out first-principles calculations to simulate Ag_2ZnSnS_4 and Ag_2CdSnS_4 and calculated enthalpies of different plausible structural models (kesterite-type, stannite-type, wurtzkesterite-type, wurtzstannite-type, and GeSb-type) to identify low- and high-pressure phases. For Ag_2ZnSnS_4, we predict the following transition: kesterite-type→[8.2GPa]→ GeSb-type. At the transition pressure, the electronic structure changes from semiconducting to metallic. For Ag_2CdSnS_4, we cannot decide which of the experimentally observed structures (kesterite-type or wurtzkesterite-type) is the ground-state structure because their energy difference is too small. At 4.7 GPa, however, we predict a transition to the GeSb-type structure with metallic character for both structures. Regarding the sensitivity of the material to disorder, a major drawback for solar cell applications, Ag_2CdSnS_4 behaves similar to Cu_2ZnSnS_4, both showing a high tendency to cationic disorder. In contrast, the disordered structures in Ag_2ZnSnS_4 are much higher in energy, and therefore, the material is less affected by disorder.

INTRODUCTION

In the research to improve solar energy conversion, one of the well-explored materials for thin-film solar cell absorbers is the direct band gap semiconductor Cu_2ZnSnS_4 (CZTS) and the corresponding selenide $Cu_2ZnSnSe_4$ (CZTSe).[1−3] The elements that make up these materials are naturally abundant and relatively environmentally friendly. Up to this point, they have shown conversion efficiencies up to 12.5%.[4,5]

On the one hand, compressive stress is of importance for the use of thin-film solar cells, as they can be sputtered. The ion bombardment in the sputtering deposition leads to compressive stress.[6,7] In CZTS(e) solar cells, either the absorber material itself is sputtered[1] or the buffer layer CdS, the transparent conducting oxide ZnO, and the antireflection coating MgF_2 layer on top are sputtered.[5] In a previous experimental and theoretical study on kesterite (KS)-type Cu_2ZnSnS_4 (Figure 1a), we have investigated the high-pressure behavior to probe its reaction to compressive stress.[8] In this study our density functional theory (DFT) calculation matched the experimental high-pressure results very well, correctly predicting an irreversible phase transition toward a metallic GeSb-type structure (Figure 1b) at 16 GPa.

In this study, we will compare the two materials Ag_2ZnSnS_4 (AZTS) and Ag_2CdSnS_4 to Cu_2ZnSnS_4 with regard to their high-pressure behavior. Ag_2ZnSnS_4 has already been tested as a solar cell absorber but shows limited efficiencies under 1% if used in a p−n homojunction.[9] The efficiency can be increased to 4.5% if the material is combined in a CZTS/AZTS heterojunction.[10] Theoretical work proposes a CdS/ACZTS/CZTS (n/p/p+) solar cell with potential efficiency close to 20%.[11] Doping $Cu_2ZnSnSe_4$ with 10% Ag leads to cells with up to 10.2% efficiency[12] revitalizing the interest in AZTS and AZTSe.[3]

Ag_2CdSnS_4 is not a suitable candidate for solar cell absorbers, as it contains Cd, which is toxic, and avoiding its use is one of the advantages of CZTS technology over better-performing CdTe thin-film solar cells. Using it in small amounts may be tolerable; doping Cu_2ZnSnS_4 with 25% Cd

Received: August 10, 2021
Accepted: September 17, 2021
Published: October 8, 2021

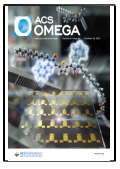

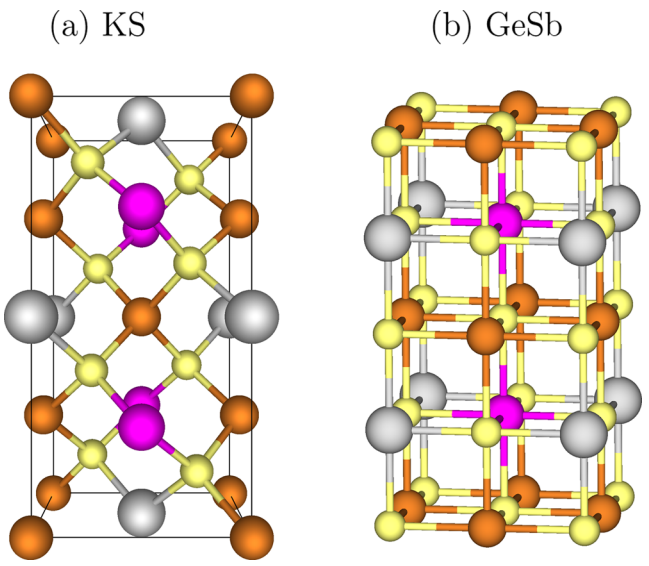

Figure 1. Structural models for (a) kesterite (KS)-type ($I\bar{4}$) and (b) GeSb-type ($P4/mmm$) Cu_2ZnSnS_4. Copper: Cu, pink: Zn, gray: Sn, and yellow: S. For the GeSb-type structure, we show two unit cells (stacked along the *c*-axis).

and 5% Ag led to cells with 10.8% efficiency.[12] Nevertheless, we include Ag_2CdSnS_4 in our study to understand the influence of the bivalent cation on high-pressure behavior.

On the other hand, one of the biggest issues with Cu_2ZnSnS_4 is Cu−Zn cationic disorder.[13,14] The main reason why Cu (ionic radius: 0.60 Å[15]) and Zn (ionic radius: 0.60 Å[15]) can be interchanged easily is their similar ionic radius. In the Ag (ionic radius: 1.00 Å[15]) analogue, Ag_2ZnSnS_4 cationic disorder is expected to be less present due to the bigger difference in the size of Ag to Zn in comparison to Cu.[16] We also include Ag_2CdSnS_4 to verify how the stability of disordered structures changes if the bivalent ion gets larger (ionic radius of Cd: 0.78 Å[15]), getting closer to the ratio present in Cu_2ZnSnS_4.

Therefore, we will apply first-principles DFT methods to investigate both, the pressure dependence of Ag_2ZnSnS_4 and Ag_2CdSnS_4 and the tendencies of the materials to cationic disorder.

COMPUTATIONAL DETAILS

Calculation Setup. The periodic density functional theory (DFT) calculations were performed with VASP 5.4.4.[17−20] A plane wave basis set with an energy cutoff of 700 eV with projector augmented wave (PAW) potentials[21,22] was used. Thus, only the valence electrons of Cu, Zn (both 4s and 3d), Ag, and Cd (both 5s and 4d) were explicitly considered. The electronic convergence criterion was set at least to 10^{-5} eV, whereby the blocked Davidson algorithm was applied as implemented in VASP. The structural relaxation of internal and external lattice parameters was set to a force convergence of 10^{-2} eV/Å^2, while the conjugate gradient algorithm implemented in VASP was used.[23] The freedom of spin polarization was enabled and a Gaussian smearing approach with a smearing factor σ of 0.01 eV was utilized. For all fully ordered structures, we simulated 16 atoms, which correspond to the number of atoms in the kesterite unit cell. The cells were fully optimized with an 8 × 8 × 4 (zinc blende (ZB)-type or GeSb-type structures) or 7 × 7 × 7 (wurtzite structures) *k*-grid constructed via the Monkhorst−Pack scheme[24] and centered at the Γ-point with the Perdew−Burke−Ernzerhof (PBE) functional.[25] On top of the PBE-optimized structures, single-point calculations for the band gap and density of states (DOS) with the HSE06-functional[26−29] were performed with a 4 × 4 × 2 (zinc blende-type or GeSb-type structures) or 4 × 4 × 4 (wurtzite-type structures) *k*-grid to account for an accurate electronic structure. The tetrahedron method with Blöchl corrections[30] was applied for the band structure evaluation. For the disordered KS structures, we fully optimized 64 atoms (equivalent to a 2 × 2 × 1 kesterite supercell) using a 4 × 4 × 4 *k*-grid.

The pressure dependence was determined by selecting volume points in a range of about 40 Å^3 above and below the minima. This corresponds to a pressure range of roughly 0−12 GPa. We used a step size of 4 Å^3, which led to at least 24 volume points for each structural model. At each point, we optimized the ionic positions and cell shape while keeping the cell volume constant. We fitted the total energy versus volume to a Birch−Murnaghan equation of state (B−M EoS).[31] Then, the pressure at each volume was obtained from the $P(V)$ formulation of the same EoS (for details, see Section S.3 in the Supporting Information). For the B−M EoS fits of the low-pressure structures, we only use data points below the transition pressure because above this pressure, the structures start to deform significantly toward the high-pressure ones. We used at least 16 volume points per fit. Using the pressure, we calculated the enthalpies ($H(P) = E + PV$) for each structural model and compared them over the investigated pressure range to identify the most stable structures.

Please note, we have not considered phonon dispersion in the different crystal structures. Based on our previous joint experimental high-pressure study on Cu_2ZnSnS_4, where our PBE calculation without phonon dispersion matched the experimental data well, we think that the influence of phonon dispersion on the transition pressure is negligible.

Structural Models. *Ordered Structures.* In quaternary chalcogenide semiconductors, the structures at equilibrium pressure in most cases are kesterite (KS)-type (Figure 2a), stannite (ST)-type (Figure 2b), wurtzkesterite (WZ-KS)-type (Figure 2c), or wurtzstannite (WZ-ST)-type (Figure 2d) structures.[32] KS and ST are derived from the zinc blende (ZB)-type structure. WZ-KS and WZ-ST are derived from the wurtzite-type structure. For the WZ structures, we use equivalent tetragonal unit cells but are aware that the asymmetric unit is hexagonal. In the tetragonal representation of the WZ cell, we can easily see the relation to the corresponding ZB-derived structure. For instance, in WZ-KS, the cationic arrangements in the *a*−*c*-planes are identical to the cationic arrangements in the *a*−*c*-planes in KS. The same relation holds for both ST structures. We include all mentioned structures as potential low-pressure phases for Ag_2ZnSnS_4 and Ag_2CdSnS_4. In our high-pressure study on KS Cu_2ZnSnS_4, we found the distorted rock salt structure (GeSb-type, Figure 1b) to be the most stable phase beyond 16 GPa. Therefore, we also include the GeSb-type structure as a high-pressure phase in this study. For the GeSb-type structure, we utilize two unit cells (stacked along the *c*-axis) so that the number of atoms matches the KS unit cell.

All ZB- and WZ-derived structures have a coordination number of 4; due to the same structural motif, they are close in formation energy and the structure formation is dependent on crystallization conditions. GeSb has a coordination number of

https://doi.org/10.1021/acsomega.1c04290
ACS Omega 2021, 6, 27387−27395

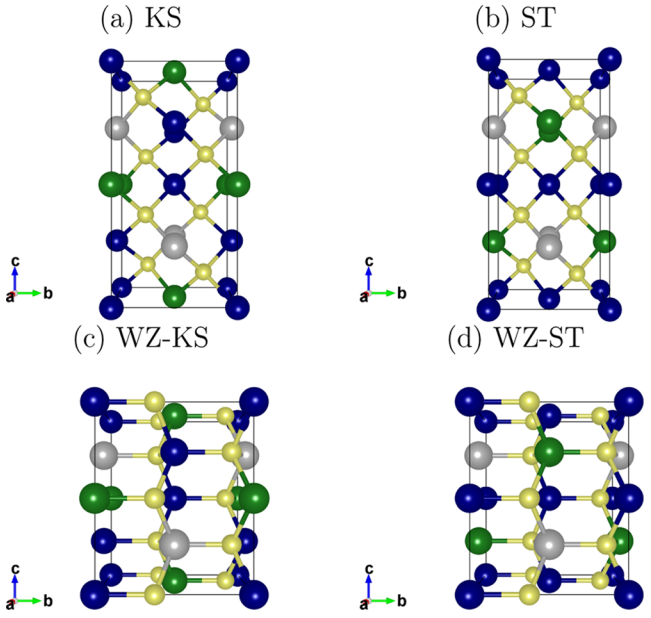

Figure 2. Structural models for the (a) kesterite (KS)-type ($I\bar{4}$), (b) stannite (ST)-type ($I\bar{4}2m$), (c) wurtzkesterite (WZ-KS)-type (Pn), and (d) wurtzstannite (WZ-ST)-type ($Pmn2_1$) structures. Blue: Ag, green: Zn/Cd, gray: Sn, and yellow: S.

6, so this structure is fundamentally different from the fourfold-coordinated ZB and WZ structures. The transition from fourfold to sixfold coordination is a structural change associated with a large difference in the energy of formation.

Please note that the optimized structures for this project have been uploaded to the NOMAD repository.[33] URL: https://dx.doi.org/10.17172/NOMAD/2021.08.03-1.

Disordered Kesterite Models. In Cu_2ZnSnS_4 (KS), Cu−Zn disorder is a common effect. The exchange is thought to only take place within the Cu−Zn planes[14,34] and is promoted by their similar ionic radii. We classify disordered structures by their disorder fraction, which we define as the number of atoms in the two Cu−Zn planes within the cell that have changed their place in comparison to the fully ordered KS structure divided by the total number of atoms of the planes. In the kesterite unit cell (Figure 1a), there are four atoms within the two Cu−Zn planes. Exchanging two of them leads to a disorder fraction of 50%. Disorder fractions above 50% lead to the same structures as for the disorder fractions below 50% due to the crystal symmetry.

The energies of all possible disorder patterns in a 2 × 2 × 1 supercell for Cu_2ZnSnS_4 were calculated to understand why disorder occurs easily and how it affects the band gap.[13,35] All possible 910 disorder patterns within this supercell have been investigated. In this study, we want to compare Ag_2ZnSnS_4 and Ag_2CdSnS_4 to Cu_2ZnSnS_4 without calculating all patterns for each material. We selected three to five patterns for each disorder fraction (Figures S.4 and S.5 in the Supporting Information) in such a way that they span the whole energy range that occurs for Cu_2ZnSnS_4.[13,35]

We do not consider disordered structures in the high-pressure part of this study because we have shown for Cu_2ZnSnS_4 that the disorder has no impact on the transition pressure.[36]

RESULTS AND DISCUSSION

Equilibrium Structures. We start by reviewing the equilibrium structures of Ag_2ZnSnS_4 and Ag_2CdSnS_4 obtained at the PBE level (Table 1) and relate them to other published results.

The mineral pirquitasite, in its ideal composition corresponding to Ag_2ZnSnS_4, was first characterized in 1982 by Johan and Picot. Based on their X-ray diffraction (XRD) measurements, they concluded that Ag_2ZnSnS_4 must have an ST or KS structure.[38] The question of which of the two ZB structures is more stable was answered in 2013 by Schumer et al.[39] Their XRD measurement indicated that Ag_2ZnSnS_4 has a KS structure at ambient pressure. These results agree with DFT calculations by Chen et al., which also predict the KS structure to be most stable.[32] In 2019, neutron diffraction measurements by Mangelis et al. proofed that ATZS has a KS structure.[37]

Our PBE calculations also predict the KS structure to be most stable (Table 1). The WZ-KS structure is only 19 meV less stable, followed by the WZ-ST structure and finally the ST structure. The PBE lattice parameters for KS match the experimental results;[37] a deviates by +0.4% and c by −3%, which we consider to be within the expected PBE error.

The crystal structure of Ag_2CdSnS_4 was first determined in the late 1960s by Parthé and Deitch. They assigned the space group $Cmc2_1$ based on their XRD results.[40] This assignment was confirmed in 2005 by Parasyuk et al., again using XRD.[41] In 2020, Heppke et al. carried out an in situ XRD study at different temperatures.[42] They found low- and high-temperature phases. For the low-temperature phase occurring below 200 °C, they excluded the space group $Cmc2_1$ due to additional reflections in their XRD pattern. Instead, they assigned WZ-KS. At 200 °C, they observed a first-order phase transition to WZ-ST.

Also, at the PBE level, the WZ-KS structure is the most stable (Table 1). But it is only 0.1 meV more stable than the KS structure; this energy difference is close to the accuracy of

Table 1. Optimized Lattice Parameters a, b, c (in Å), and β (in deg) for Ag_2BSnS_4 (B: Zn, Cd) KS, ST, WZ-KS, and WZ-ST at the PBE Level of Theory in Comparison to Other Simulated and Experimental (Exp.) Results[a]

	KS			ST			WZ-KS					WZ-ST				
B	a	c	ΔE	a	c	ΔE	a	b	c	β	ΔE	a	b	c	ΔE	method
Zn	5.835	11.088	0	5.564	12.177	293	6.665	6.922	8.197	89.98	32	7.831	7.200	6.695	172	PBE
	5.812	10.779														exp.[37]
			0			298					19				162	PW91[32]
Cd	5.910	11.560	0	5.803	11.975	95	6.807	7.150	8.303	90.07	0	8.147	7.260	6.820	40	PBE
							6.704	7.037	8.217	90.16		8.217	7.064	6.703		exp.[37]
			14			117					0				38	PW91[32]

[a] ΔE denotes the energy difference per unit cell to the most stable phase (in meV).

https://doi.org/10.1021/acsomega.1c04290
ACS Omega 2021, 6, 27387−27395

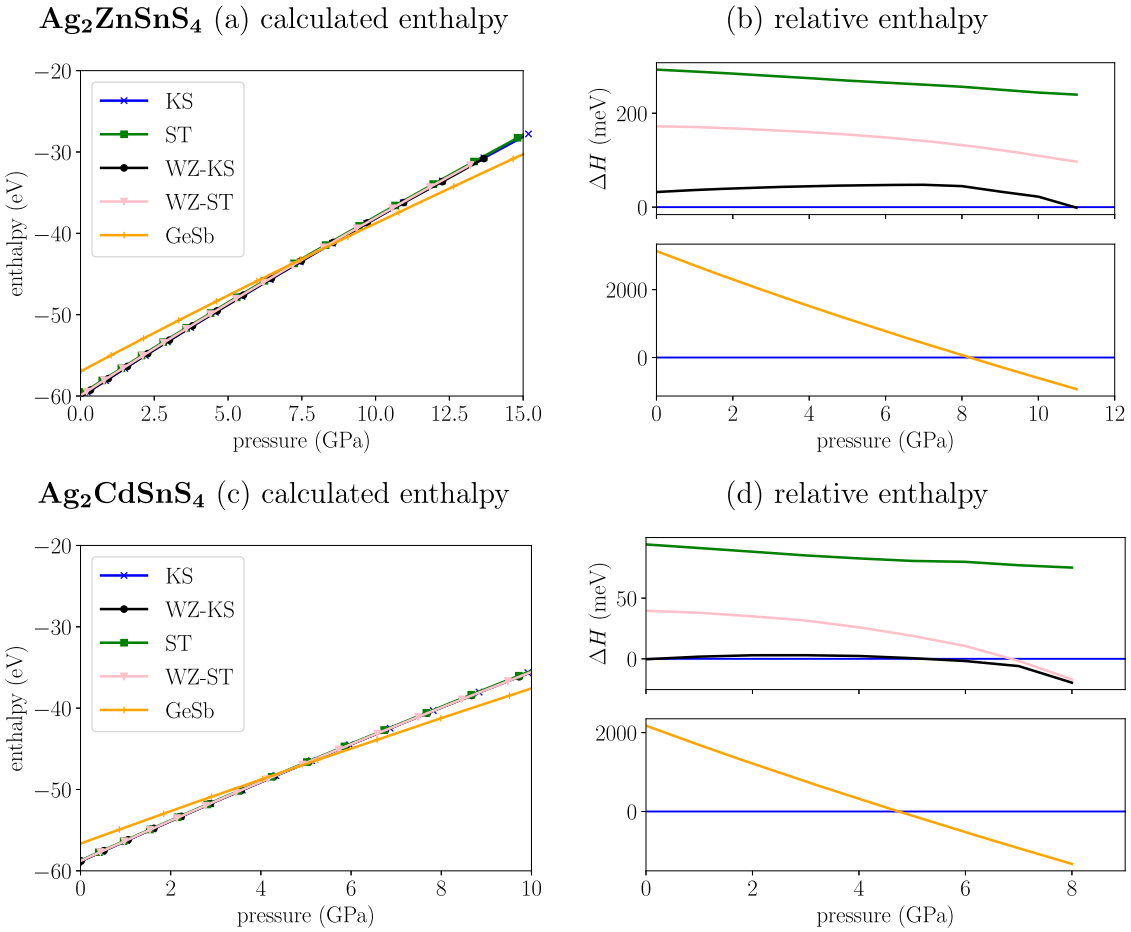

Figure 3. (a, c) PBE-calculated enthalpies for KS-, ST-, WZ-KS-, WZ-ST-, and GeSb-type structural models as a function of pressure for Ag_2ZnSnS_4 and Ag_2CdSnS_4. Because the enthalpy differences are very small, we also calculated relative enthalpy differences (b, d) with reference to the most stable structure for Ag_2ZnSnS_4 and Ag_2CdSnS_4.

our calculations, so we cannot predict which of the two structures is more stable. The WZ-ST and ST structures are 38 and 117 meV less stable than the KS structures at the PBE level, respectively.

The DFT results are in agreement with the assignment of WZ-KS to the low-temperature phase of Ag_2CdSnS_4 by Heppke et al.[42] The PBE lattice parameter for WZ-KS is around 1.5% of the experimental results. For WZ-ST, the deviations are similar, except for *b*, where we observe a deviation of about 3%. We consider this agreement to be within the error of the applied functional.

The predicted relative stability at the PBE level for both materials closely matches the PW91 results by Chen et al.,[32] and only the difference in energy between KS and WZ-KS is more pronounced. The WZ-KS structure is 14 meV more stable than KS at the PW91 level.

The similarity of the DFT results is not surprising, as both DFT functionals are from the same class of functionals, and they use a generalized gradient approximation (GGA) for the exchange−correlation potential.[25]

High-Pressure Behavior. The high-pressure behavior gives hints of how the materials perform structurally in thin-layer solar cells, where compressive stress occurs. For instance, in 300 nm thin TiN films, compressive stress can amount up to 4 GPa.[43] Plotting the enthalpies for Ag_2ZnSnS_4 (Figure 3a,b) and Ag_2CdSnS_4 (Figure 3c,d), we find that the KS structure stays most stable until 8.2 and 4.7 GPa, respectively. At these pressures, we predict a transition to the GeSb-type structure for both materials. This transition leads to the shrinking of the unit cell by 16% for Ag_2ZnSnS_4 and 18% for Ag_2CdSnS_4. In Ag_2ZnSnS_4, the low pressure stability is unambiguous, and the energy difference from the most stable KS structure to the second most stable WZ-KS structure is constantly around 40 meV until the transition pressure and afterward decreases to eventually become less stable around 11 GPa, which has no effect on the experimental findings because it is well above the transition pressure to the GeSb-type structure. For Ag_2CdSnS_4 KS and WZ-KS, the enthalpies are similar up to the transition pressure. The maximum difference is 3 meV at 2.8 GPa. We estimated the error in ΔH (for details, see Section S.4 in the Supporting Information) and came to the conclusion that the differences in enthalpy between KS and WZ-KS are not significant up to the transition. Consequently, we cannot decide which of the two structures is more stable at low pressures for Ag_2CdSnS_4. As mentioned above, experimentally, the WZ-KS structure is observed at low pressure.[42] At 6.4 GPa, WZ-KS also becomes more stable in our calculations, but this cannot be observed experimentally, as it is beyond the transition pressure for the GeSb-type structure.

In Ag_2ZnSnS_4, the relative stability of all low-pressure phases remains close to the stability at ambient conditions up to the transition pressure. For Ag_2ZnSnS_4 ST and WZ-ST, the energy difference to KS at the transition pressure is 30 and 40 meV smaller than at ambient pressure, respectively. In Ag_2CdSnS_4,

https://doi.org/10.1021/acsomega.1c04290
ACS Omega 2021, 6, 27387−27395

the enthalpy of the ST phase slowly decreases from 100 to 80 meV above the KS enthalpy. The enthalpy of WZ-ST Ag_2CdSnS_4 decreases from 50 meV above KS at ambient pressure to become more stable around 6.5 GPa, which is beyond the transition pressure to the GeSb structure.

Now, we compare the predicted phase transitions for the two Ag KS/WZ-KS to the phase transition in Cu_2ZnSnS_4 (Table 2). Exchanging Cu for Ag leads to a reduction of the transition pressure nearly by a factor of 2. Additionally, exchanging Zn for Cd leads to another 1.75-fold decrease of the transition pressure. The relative volume change due to the pressure-induced transition, however, is around 3.1% in all materials, so quite similar. With reference to the resistance against stress, we conclude that Ag_2ZnSnS_4 and Ag_2CdSnS_4 are significantly less resistant than Cu_2ZnSnS_4. Still, Ag_2ZnSnS_4 seems suitable for use in thin-film solar cells, as its transition pressure is 2 times larger than the maximum compressive stress of 4 GPa expected in thin films.[43] The transition pressure of Ag_2CdSnS_4, however, is only 0.7 GPa larger than the maximum compressive stress in thin films. We conclude that this could lead to unwanted structural changes in very thin Ag_2CdSnS_4 films.

Table 2. Predicted Transitions for Ag_2ZnSnS_4 and Ag_2CdSnS_4 in Comparison to Experimental Transition for Cu_2ZnSnS_4.[a]

composition	p_T	transition	V_1	V_2	ΔV (%)
Ag_2ZnSnS_4	8.2	KS → GeSb	337	282	−16.3
Ag_2CdSnS_4	4.7	WZ-KS/KS → GeSb	374	306	−18.0
Cu_2ZnSnS_4[8]	16.0	KS → GeSb	280	240	−15.2

[a]The table contains the transition pressure (p_T in GPa) with the corresponding cell volume before (V_1 in Å^3) and after (V_2 in Å^3) the transition. ΔV denotes the relative volume change.

We want to analyze how the bulk modulus changes due to the phase transitions in the materials Ag_2ZnSnS_4 and Ag_2CdSnS_4 and compare to Cu_2ZnSnS_4. We do that based on the B−M EoS fit coefficients, as the bulk modulus and its first derivative are variables in the EoS. The bulk moduli of the low-pressure structures amount to 81% for Ag_2ZnSnS_4 and 73−75% for Ag_2CdSnS_4 of the bulk modulus of KS Cu_2ZnSnS_4 (Table 3). By comparing the different materials at low pressure, the bulk moduli reflect different transition pressures. The lower the bulk modulus, the lower the transition pressure.

Table 3. PBE Reference Volume per KS-Sized Unit Cell (V_0 in Å^3), Bulk Modulus (B_0 in GPa), and the First Derivative (B_0') for the Listed Structural Models (Struc.) for the Listed Compositions[a]

composition	struc.	V_0	B_0	B_0'
Ag_2ZnSnS_4	KS	377.59	54.71	4.96
Ag_2ZnSnS_4	GeSb	308.06	75.84	4.68
Ag_2CdSnS_4	WZ-KS	404.12	49.50	5.10
Ag_2CdSnS_4	KS	403.68	50.69	5.20
Ag_2CdSnS_4	GeSb	323.77	71.72	4.83
Cu_2ZnSnS_4[8]	KS	307.50	68.63	4.64
Cu_2ZnSnS_4[8]	GeSb	241.50	82.16	4.57

[a]Derived from the Birch−Murnaghan EoS fit. For all fit parameters, please refer to Section S.3 in the Supporting Information. For error estimates and coefficients, please refer to Tables S.7 and S.10 in the Supporting Information.

The bulk moduli of the GeSb-type high-pressure structures amount to 92% for Ag_2ZnSnS_4 and 88% for Ag_2CdSnS_4 of the bulk modulus of GeSb-type Cu_2ZnSnS_4. The first derivative of the bulk modulus is within 10% for all materials and structures. For all materials, B_0' of the GeSb-type structure is smaller than those for the low-pressure phases.

Electronic Structure at Ambient and High Pressure. For materials to be used as solar cell absorbers, the size of their band gap is crucial. Therefore, we investigated the electronic band structure for equilibrium and high-pressure structures for both compounds with the HSE06 hybrid functional.[26]

The results for the band gap at equilibrium pressure for KS Ag_2ZnSnS_4 and WZ-KS Ag_2ZnSnS_4 are very similar. In both cases, we predict a band gap of 1.5 eV (Table 4). The experimentally observed band gaps are 2.0[44] and 1.93 eV, respectively.[42] Considering that HSE06 usually gives very accurate band gaps, a deviation of 0.5 eV seems large. We are confident that the reason for the large deviation is mainly that we did not optimize our structures at the HSE06 level but only with PBE. We have encountered this phenomenon before while studying Cu_2ZnSnS_4.[35] In Cu_2ZnSnS_4, the HSE band gap of the PBE-optimized structure is 1.2 eV. If we also optimize with HSE06 the band gap increases to 1.5 eV. Given this experience in previous studies, we do not reoptimize the structures at the HSE06 level here and assume a similar behavior. With a correction term of ca. +0.3 eV, the band gap values show reasonable agreement with the experiment.

Table 4. Calculated HSE06 Band Gaps (Single-Point Calculations for the Optimized PBE Structures) E_g (in eV) for Ag_2CdSnS_4 and Ag_2CdSnS_4 for the Listed Structural Models (Struc.) in Comparison to the Experimental (Exp.) Results

composition	struc.	E_g	exp.
Ag_2ZnSnS_4	KS	1.5	2.0[44]
Ag_2ZnSnS_4	WZ-KS	1.6	
Ag_2ZnSnS_4	WZ-ST	1.4	
Ag_2ZnSnS_4	ST	1.2	
Ag_2CdSnS_4	WZ-KS	1.5	1.93[42]
Ag_2CdSnS_4	WZ-ST	1.3	
Ag_2CdSnS_4	KS	1.4	
Ag_2CdSnS_4	ST	1.2	

To test if the band gap is a suitable criterion to distinguish the different structures for each material, we also calculated the band gaps for all other structural models (Table 4). For Ag_2ZnSnS_4, we predict the band gaps of all structures within an interval of 0.3 eV; for Ag_2CdSnS_4, the interval is 0.4 eV. Within these intervals, the differences between the structures are 0.1 or 0.2 eV. We consider these differences as too small to distinguish them based on experimental band gaps. The reason for the similar band gaps is that all ZB and WZ structures have a tetrahedral binding motif around sulfur anions; therefore, the chemical bonding situation is similar and also the resulting DOS (see Section S.5.2 in the Supporting Information).

To analyze how the electronic structure changes due to the pressure-induced transition, we calculated the DOS at the transition pressure for the low- and high-pressure structures for Ag_2ZnSnS_4 and Ag_2CdSnS_4 (Figure 4). The results for both materials are very similar; we find that the band gap in KS or WZ-KS closes completely after the transition to GeSb. We observe that all bands from the valence band now extend in the

https://doi.org/10.1021/acsomega.1c04290
ACS Omega 2021, 6, 27387−27395

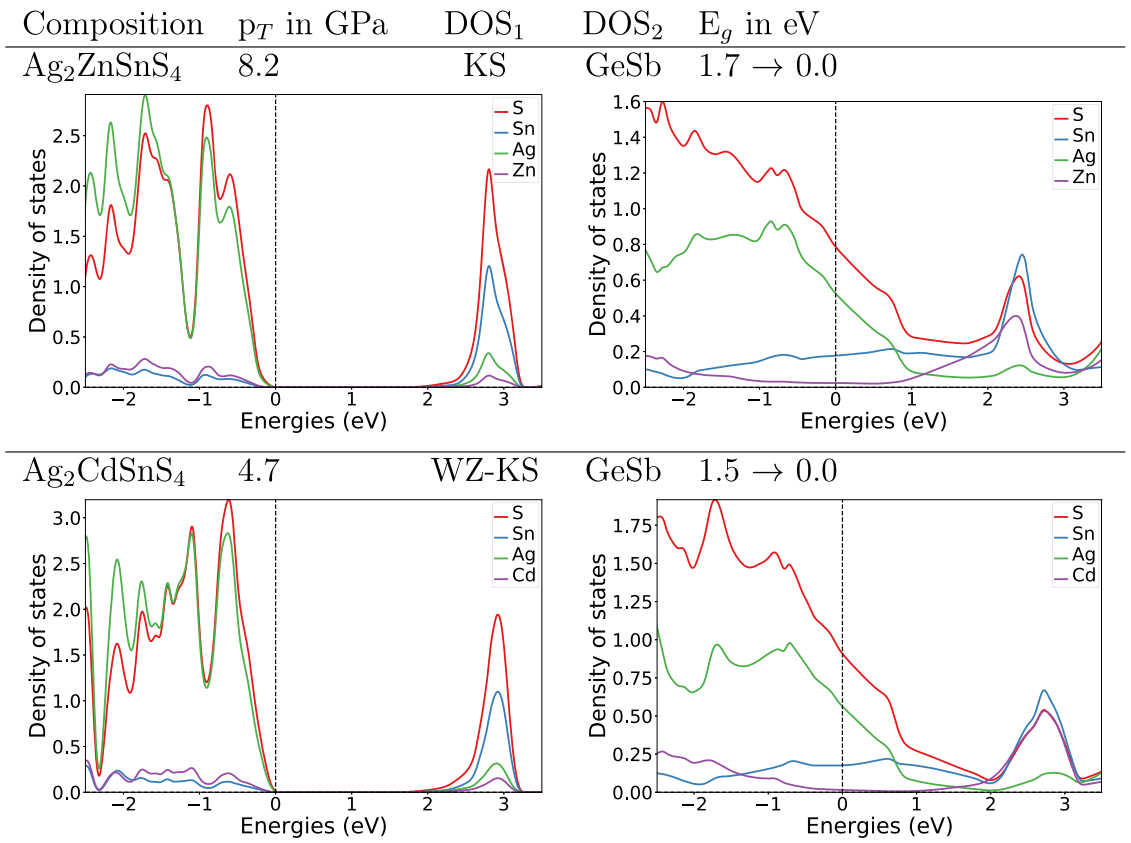

Figure 4. DOS plots at the transition pressure at the HSE06 level for the listed pressure-induced transitions for Ag_2ZnSnS_4 and Ag_2CdSnS_4.

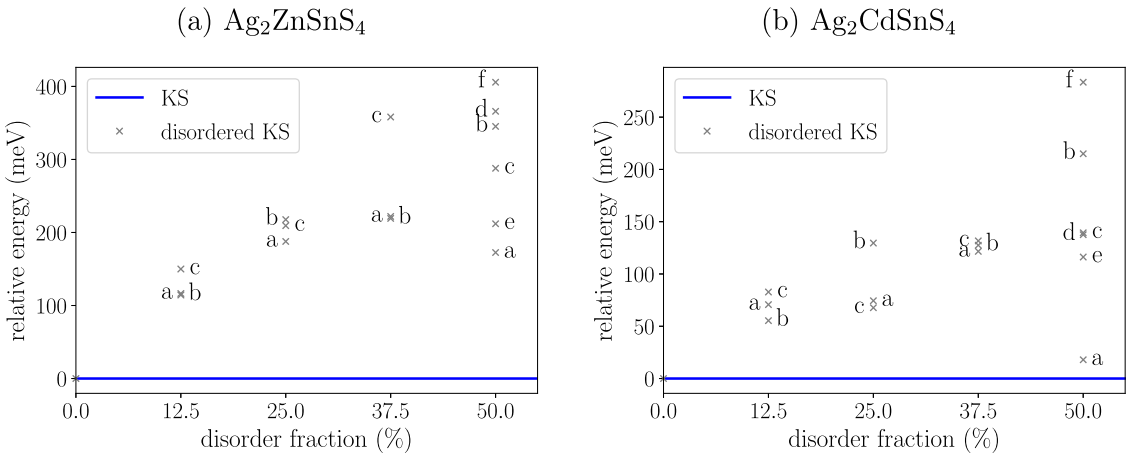

Figure 5. Relative PBE energies of disordered KS structures with reference to ideal KS for (a) Ag_2ZnSnS_4 and (b) Ag_2CdSnS_4. For Cu_2ZnSnS_4, please refer to Figure S.6 in the Supporting Information.

region from 0 to 1.5 eV, which is the band gap region for the KS or WZ-KS structure. The electronic structure changes from semiconducting to metallic for both materials. Before the transition, the band gap in KS Ag_2ZnSnS_4 widens by 0.2 eV in comparison to equilibrium pressure. For Ag_2CdSnS_4, we plotted the DOS for WZ-KS for the low-pressure phase because the XRD experiments by Heppke et al.[42] indicate it as the equilibrium pressure structure. For Ag_2CdSnS_4 WZ-KS, the band gap does not widen prior to the transition. We suspect that this is because the transition takes place at a 3 GPa lower pressure than that in KS Ag_2ZnSnS_4. We are confident that the results would be the same if we use a KS Ag_2CdSnS_4 low-pressure phase because DOSs are nearly identical at equilibrium pressure.

Disorder. We restrict our investigations to the KS structure because it is the most stable phase for Ag_2ZnSnS_4 and Cu_2ZnSnS_4. Although the situation is not as defined in Ag_2CdSnS_4, the KS structure is one of the two possibilities of the low-pressure phases. Also, it can give an indication of how doping KS Cu_2ZnSnS_4 with Ag and Cd together[12] influences disorder.

To predict how sensitive the materials Ag_2ZnSnS_4 and Ag_2CdSnS_4 are toward disorder, we calculated at least three disordered structures for each disorder fraction within 2 × 2 × 1 super cells. The relative energies with respect to the ideal KS

https://doi.org/10.1021/acsomega.1c04290
ACS Omega 2021, 6, 27387−27395

structure (Figure 5a,b) are compared to the ones of Cu_2ZnSnS_4 (Figure S.6 in the Supporting Information). It is observed that the results for Ag_2CdSnS_4 and Cu_2ZnSnS_4 are nearly identical with relative energies ranging from 20 to 270 meV. The relative energy order of the patterns within each disorder fraction is the same, except for small deviations for disorder fractions of 37.5 and 50%. Also, the relative energies themselves for each pattern are similar in Ag_2CdSnS_4 and Cu_2ZnSnS_4. Also, it is observed that in both materials, there is a disorder pattern with 50% disorder (pattern (a), Figure S.5 in the Supporting Information), which is less than 20 meV above the ideal KS. In this pattern (space group $P\bar{4}2c$), both Ag−Cd planes are symmetrical with respect to the middle Ag−Sn plane of the cell. This pattern is very similar to KS itself, as it can be obtained by rotating the lower half of the KS unit cell (Figure 2a) by 90° (or by switching Ag and Cd in the lower Ag−Cd plane). For Ag_2CdSnS_4 and Cu_2ZnSnS_4, there are five disorder patterns with relative energies under 100 meV including pattern (a) at a disorder fraction of 50%, which is nearly as stable as ideal KS.

For Ag_2ZnSnS_4, all relative energies are higher than those for the other two, ranging from 100 to 400 meV. For disorder fractions of 25.0, 37.5, and 50%, the order of the patterns is different from those for Cu_2ZnSnS_4 and Ag_2CdSnS_4. Some patterns get significantly destabilized in comparison to the other two materials, and these are patterns (a) and (c) at a disorder fraction of 25.0%, pattern (c) at a disorder fraction of 37.5%, and patterns (a), (c), and (d) at a disorder fraction of 50%.

Cu_2ZnSnS_4 is known to be affected by cationic disorder, and based on the relative energies of the disordered structures, we expect the same for Ag_2CdSnS_4. All disordered structures for Ag_2ZnSnS_4, however, are at least 100 meV above ideal KS, and therefore, we predict that this material is much less sensitive to disorder than the other two. DFT calculations for Ag_2ZnSnS_4 by Mangelis et al. where only five disorder patterns were considered to indicate the same result.[37]

SUMMARY AND CONCLUSIONS

We simulated the enthalpies for different structural models for Ag_2ZnSnS_4 and Ag_2CdSnS_4 to identify low- and high-pressure modifications. In agreement with the experimental results, we found the tetrahedrally coordinated KS structure to be most stable for Ag_2ZnSnS_4 at equilibrium pressure. At 8.2 GPa, we predict a transition to the sixfold-coordinated GeSb-type structure. This is accompanied by a change in the electronic structure from semiconducting to metallic. For Ag_2CdSnS_4, the situation is not so clear. Numerically, we get the same result as Heppke et al. in their XRD measurements at a low temperature[42] that WZ-KS is most stable. The difference to the next least stable KS structure is only 0.1 meV, which we consider too small in comparison to the error of our calculations to determine which structure is more stable. Beyond 4.7 GPa, we found the GeSb-type structure to be undoubtedly the most stable one. The transition also leads to a change in the electronic structure from semiconducting to metallic. Also, in Cu_2ZnSnS_4, we find a metallic GeSb-type high-pressure phase; a transition pressure of 16 GPa, however, is larger by factors of 2 for Ag_2ZnSnS_4 and 3 for Ag_2CdSnS_4.

Compressive stress in thin films can amount up to 4 GPa in TiN films.[43] Assuming similar behavior for thin films of the investigated materials, we conclude that Ag_2ZnSnS_4 and Cu_2ZnSnS_4 are sufficiently resistant to compressive stress. The transition pressure of Ag_2CdSnS_4 is close to the maximum compressive stress in TiN thin films; therefore, it could become critical for the usage in very thin films. If the WZ-KS or KS to GeSb-type transition is triggered, the material is rendered useless as a solar cell absorber due to the metallic electronic structure of the GeSb-type structure.

By calculating differently disordered KS patterns, we also revealed that KS Ag_2CdSnS_4 is similarly prone to disorder as KS Cu_2ZnSnS_4. The reason is that the ionic radii of Cu^+ and Zn^{2+} are relatively similar as well as the ionic radii of Ag^+ and Cd^{2+}. These elements constitute two planes in the KS unit cell, which can easily get disordered if the elements are similar in size. In Ag_2ZnSnS_4, the effective ionic radii of the elements are sufficiently different for the disordered structures to be destabilized by 50−150 meV each in comparison to Cu_2ZnSnS_4 and Ag_2CdSnS_4. We conclude that Ag_2ZnSnS_4 is much less sensitive to disorder.

ASSOCIATED CONTENT

Supporting Information

The Supporting Information is available free of charge at https://pubs.acs.org/doi/10.1021/acsomega.1c04290.

All DFT energies and structural data; B−M fit parameter; error estimation ΔH; additional DOS; disordered KS models; and CZTS data for comparison (PDF)

AUTHOR INFORMATION

Corresponding Author

Tim Küllmey − *Institut für Chemie und Biochemie, Freie Universität Berlin, 14195 Berlin, Germany;* orcid.org/0000-0002-3848-3015; Email: tim.kuellmey@fu-berlin.de

Authors

Jakob Hein − *Institut für Chemie und Biochemie, Freie Universität Berlin, 14195 Berlin, Germany*

Eva M. Heppke − *Institut für Chemie, Technische Universität Berlin, 10623 Berlin, Germany*

Ilias Efthimiopoulos − *Section 3.6: Chemistry and Physics of Earth Materials, Deutsches GeoForschungsZentrum (GFZ), 14473 Potsdam, Germany; Institute of Physics, University of Greifswald, 17489 Greifswald, Germany;* orcid.org/0000-0001-6542-8188

Beate Paulus − *Institut für Chemie und Biochemie, Freie Universität Berlin, 14195 Berlin, Germany*

Complete contact information is available at: https://pubs.acs.org/10.1021/acsomega.1c04290

Notes

The authors declare no competing financial interest.

ACKNOWLEDGMENTS

The authors acknowledge the North-German Supercomputing Alliance (HLRN) for providing high-performance computing (HPC) resources that have contributed to the research results reported in this paper. Financial support from International Max Planck Research School (IMPRS) Functional Interfaces in Physics and Chemistry is gratefully acknowledged.

REFERENCES

(1) Tanaka, T.; Nagatomo, T.; Kawasaki, D.; Nishio, M.; Guo, Q.; Wakahara, A.; Yoshida, A.; Ogawa, H. Preparation of Cu_2ZnSnS_4 thin films by hybrid sputtering. *J. Phys. Chem. Solids* **2005**, *66*, 1978−1981.

(2) Scragg, J. J.; Dale, P. J.; Peter, L. M.; Zoppi, G.; Forbes, I. New routes to sustainable photovoltaics: Evaluation of Cu_2ZnSnS_4 as an alternative absorber material. *Phys. Status Solidi B* **2008**, *245*, 1772−1778.

(3) Giraldo, S.; Jehl, Z.; Placidi, M.; Izquierdo-Roca, V.; Pérez-Rodríguez, A.; Saucedo, E. Progress and Perspectives of Thin Film Kesterite Photovoltaic Technology: A Critical Review. *Adv. Mater.* **2019**, *31*, No. 1806692.

(4) Yan, C.; et al. Cu_2ZnSnS_4 solar cells with over 10% power conversion efficiency enabled by heterojunction heat treatment. *Nat. Energy* **2018**, *3*, 764−772.

(5) Wang, W.; Winkler, M. T.; Gunawan, O.; Gokmen, T.; Todorov, T. K.; Zhu, Y.; Mitzi, D. B. Device characteristics of CZTSSe thin-film solar cells with 12.6% efficiency. *Adv. Energy Mater.* **2014**, *4*, No. 1301465.

(6) Janssen, G. C. Stress and strain in polycrystalline thin films. *Thin Solid Films* **2007**, *515*, 6654−6664.

(7) Windischmann, H. Intrinsic stress in sputter-deposited thin films. *Crit. Rev. Solid State Mater. Sci.* **1992**, *17*, 547−596.

(8) Efthimiopoulos, I.; Küllmey, T.; Speziale, S.; Pakhomova, A. S.; Quennet, M.; Paulus, B.; Ritscher, A.; Lerch, M.; Koch-Müller, M. Pressure-induced structural and electronic transitions in kesterite-type Cu_2ZnSnS_4. *J. Appl. Phys.* **2018**, *124*, No. 085905.

(9) Ma, C.; Guo, H.; Zhang, K.; Li, Y.; Yuan, N.; Ding, J. The preparation of Ag_2ZnSnS_4 homojunction solar cells. *Mater. Lett.* **2017**, *207*, 209−212.

(10) Guo, H.; Ma, C.; Zhang, K.; Jia, X.; Li, Y.; Yuan, N.; Ding, J. The fabrication of Cd-free Cu_2ZnSnS_4-Ag_2ZnSnS_4 heterojunction photovoltaic devices. *Sol. Energy Mater. Sol. Cells* **2018**, *178*, 146−153.

(11) Saha, U.; Alam, M. K. Boosting the efficiency of single junction kesterite solar cell using Ag mixed Cu_2ZnSnS_4 active layer. *RSC Adv.* **2018**, *8*, 4905−4913.

(12) Gershon, T.; Lee, Y. S.; Antunez, P.; Mankad, R.; Singh, S.; Bishop, D.; Gunawan, O.; Hopstaken, M.; Haight, R. Photovoltaic materials and devices based on the alloyed kesterite absorber $(Ag_xCu_{1-x})_2Zn(Sn,Se)_4$. *Adv. Energy Mater.* **2016**, *6*, No. 1502468.

(13) Quennet, M.; Ritscher, A.; Lerch, M.; Paulus, B. The order-disorder transition in Cu_2ZnSnS_4: A theoretical and experimental study. *J. Solid State Chem.* **2017**, *250*, 140−144.

(14) Scragg, J. J. S.; Larsen, J. K.; Kumar, M.; Persson, C.; Sendler, J.; Siebentritt, S.; Platzer Björkman, C. Cu-Zn disorder and band gap fluctuations in Cu2ZnSn(S,Se)4: Theoretical and experimental investigations. *Phys. Status Solidi B* **2016**, *253*, 247−254.

(15) Shannon, R. D. Revised effective ionic radii and systematic studies of interatomic distances in halides and chalcogenides. *Acta Crystallogr., Sect. A* **1976**, *32*, 751−767.

(16) Ma, C.; Guo, H.; Zhang, K.; Yuan, N.; Ding, J. Fabrication of p-type kesterite Ag_2ZnSnS_4 thin films with a high hole mobility. *Mater. Lett.* **2017**, *186*, 390−393.

(17) Kresse, G.; Hafner, J. Ab initiomolecular dynamics for liquid metals. *Phys. Rev. B* **1993**, *47*, 558−561.

(18) Kresse, G.; Hafner, J. Ab initiomolecular-dynamics simulation of the liquid-metal-amorphous-semiconductor transition in germanium. *Phys. Rev. B* **1994**, *49*, 14251−14269.

(19) Kresse, G.; Furthmüller, J. Efficient iterative schemes forab initiototal-energy calculations using a plane-wave basis set. *Phys. Rev. B* **1996**, *54*, 11169−11186.

(20) Kresse, G.; Furthmüller, J. Efficiency of ab-initio total energy calculations for metals and semiconductors using a plane-wave basis set. *Comput. Mater. Sci.* **1996**, *6*, 15−50.

(21) Blöchl, P. Projector augmented-wave method. *Phys. Rev. B* **1994**, *50*, 17953−17979.

(22) Kresse, G.; Joubert, D. From ultrasoft pseudopotentials to the projector augmented-wave method. *Phys. Rev. B* **1999**, *59*, 1758−1775.

(23) Ziegel, E. Numerical Recipes: The Art of Scientific Computing. *Technometrics* **1987**, *29*, 501.

(24) Monkhorst, H. J.; Pack, J. D. Special points for Brillouin-zone integrations. *Phys. Rev. B* **1976**, *13*, 5188−5192.

(25) Perdew, J. P.; Burke, K.; Ernzerhof, M. Generalized Gradient Approximation Made Simple. *Phys. Rev. Lett.* **1996**, *77*, 3865−3868.

(26) Heyd, J.; Scuseria, G. E.; Ernzerhof, M. Hybrid functionals based on a screened Coulomb potential. *J. Chem. Phys.* **2003**, *118*, 8207−8215.

(27) Heyd, J.; Scuseria, G. E. Efficient hybrid density functional calculations in solids: Assessment of the Heyd-Scuseria-Ernzerhof screened Coulomb hybrid functional. *J. Chem. Phys.* **2004**, *121*, 1187−1192.

(28) Heyd, J.; Scuseria, G. E.; Ernzerhof, M. Erratum: "Hybrid functionals based on a screened Coulomb potential" [J. Chem. Phys. 118, 8207 (2003)]. *J. Chem. Phys.* **2006**, *124*, No. 219906.

(29) Krukau, A. V.; Vydrov, O. A.; Izmaylov, A. F.; Scuseria, G. E. Influence of the exchange screening parameter on the performance of screened hybrid functionals. *J. Chem. Phys.* **2006**, *125*, No. 224106.

(30) Blöchl, P. E.; Jepsen, O.; Andersen, O. Improved tetrahedron method for Brillouin-zone integrations. *Phys. Rev. B* **1994**, *49*, 16223−16233.

(31) Birch, F. Finite Elastic Strain of Cubic Crystals. *Phys. Rev.* **1947**, *71*, 809−824.

(32) Chen, S.; Walsh, A.; Luo, Y.; Yang, J. H.; Gong, X. G.; Wei, S. H. Wurtzite-derived polytypes of kesterite and stannite quaternary chalcogenide semiconductors. *Phys. Rev. B: Condens. Matter Mater. Phys.* **2010**, *82*, No. 195203.

(33) Draxl, C.; Scheffler, M. NOMAD: The FAIR concept for big data-driven materials science. *MRS Bull.* **2018**, *43*, 676−682.

(34) Bourdais, S.; Choné, C.; Delatouche, B.; Jacob, A.; Larramona, G.; Moisan, C.; Lafond, A.; Donatini, F.; Rey, G.; Siebentritt, S.; Walsh, A.; Dennler, G. Is the Cu/Zn Disorder the Main Culprit for the Voltage Deficit in Kesterite Solar Cells? *Adv. Energy Mater.* **2016**, *6*, No. 1502276.

(35) Quennet, M. First Principles Calculations for the Semiconductor Material Kesterite Cu_2ZnSnS_4 and Se-containing Derivatives. Ph.D. Thesis, Freie Universität Berlin, 2016.

(36) Efthimiopoulos, I.; Küllmey, T.; Speziale, S.; Pakhomova, A. S.; Quennet, M.; Paulus, B.; Ritscher, A.; Lerch, M. High-pressure behavior of disodered kesterite-type Cu_2ZnSnS_4. *Appl. Phys. A: Mater. Sci. Process.* **2021**, *127*, No. 616.

(37) Mangelis, P.; Aziz, A.; Da Silva, I.; Grau-Crespo, R.; Vaqueiro, P.; Powell, A. V. Understanding the origin of disorder in kesterite-type chalcogenides A_2ZnBQ_4 (A = Cu, Ag; B = Sn, Ge; Q = S, Se): The influence of inter-layer interactions. *Phys. Chem. Chem. Phys.* **2019**, *21*, 19311−19317.

(38) Johan, Z.; Picot, P. La pirquitasite, Ag_2ZnSnS_4, un nouveau membre du groupe de la stannite. *Bull. Mineral.* **1982**, *105*, 229−235.

(39) Schumer, B. N.; Downs, R. T.; Domanik, K. J.; Andrade, M. B.; Origlieri, M. J. Pirquitasite, Ag_2ZnSnS_4. *Acta Crystallogr., Sect. E: Struct. Rep. Online* **2013**, *69*, i8−i9.

(40) Parthé, E.; Yvon, K.; Deitch, R. H. The crystal structure of Cu_2CdGeS_4 and other quaternary normal tetrahedral structure compounds. *Acta Crystallogr., Sect. B: Struct. Crystallogr. Cryst. Chem.* **1969**, *25*, 1164−1174.

(41) Parasyuk, O. V.; Olekseyuk, I. D.; Piskach, L. V.; Volkov, S. V.; Pekhnyo, V. I. Phase relations in the Ag_2S-CdS-SnS_2 system and the crystal structure of the compounds. *J. Alloys Compd.* **2005**, *399*, 173−177.

(42) Heppke, E. M.; Berendts, S.; Lerch, M. Crystal structure of mechanochemically synthesized Ag_2CdSnS_4. *Z. Naturforsch. B* **2020**, *75*, 393−402.

(43) Köstenbauer, H.; Fontalvo, G. A.; Kapp, M.; Keckes, J.; Mitterer, C. Annealing of intrinsic stresses in sputtered TiN films: The role of thickness-dependent gradients of point defect density. *Surf. Coat. Technol.* **2007**, *201*, 4777−4780.

(44) Gong, W.; Tabata, T.; Takei, K.; Morihama, M.; Maeda, T.; Wada, T. Crystallographic and optical properties of $(Cu,Ag)_2ZnSnS_4$

https://doi.org/10.1021/acsomega.1c04290
ACS Omega 2021, 6, 27387−27395

and $(Cu,Ag)_2ZnSnSe_4$ solid solutions. *Phys. Status Solidi C* **2015**, *12*, 700−703.

https://doi.org/10.1021/acsomega.1c04290
ACS Omega 2021, 6, 27387−27395